Int. J. Multiphase Flow Vol. 15, No. 4, pp. 505–520, 1989
Printed in Great Britain.

0301-9322/89 $3.00 + 0.00

MODELLING OF WAVY FLOW IN TURBULENT FREE FALLING FILMS

N. BRAUNER
Department of Fluid Mechanics and Heat Transfer, School of Engineering, Tel Aviv University, Ramat Aviv 69978, Israel

(*Received* 15 *May* 1987; *in revised form* 25 *December* 1988)

Abstract—Turbulent wavy flow models for intermediate and high Re are presented. The modelling is based on different mechanisms which control the various zones along the wave. It is shown that sufficient information may be available to generate a closed-form solution. Reasonably satisfactory agreement between the theoretical predictions and the experiments is obtained for a wide range of film Re.

Key Words: thin, falling films, waves, turbulence, annular flow

1. INTRODUCTION

The wavy pattern in developed downward wavy film flow is characterized by the existence of highly disturbed lumps of liquid, travelling downstream over a thin substrate film at a velocity which is several times larger than the mean velocity of the substrate film. These rolling large waves are the cause of the substantial increase observed in transport rates of momentum heat and mass across wavy liquid films.

The modelling of wavy flow has been traditionally tackled by solving the highly nonlinear equations of motion over the entire length of a single wave. The many attempts, which did start with a single solution strategy for the whole wave unit, could provide only partial information on the associated physical mechanisms and, in principle, none of these could lead to a complete closed-form solution.

A different approach has been offered by Brauner & Moalem Maron (1983) and Moalem Maron *et al.* (1985), whereby the wave is viewed as a composite of series of zones, each of which has its own characteristic mechanisms and a corresponding solution strategy. Thus, the equations of motion are solved for each zone and the solutions are matched at the junctions between the different sections of the wave. The model has been extended to account for cocurrent (Brauner *et al.* 1985) and countercurrent (Brauner *et al.* 1987b) interfacial shear. However, these models are restricted to relatively low film Reynolds numbers where the entire flow field is laminar.

As has been shown previously (Brauner & Moalem Maron 1983; Moalem Maron *et al.* 1985), the major part of the flow rate is carried by the rolling liquid lumps, while the thin substrate film, which separates the waves, carries only 10^{-1} of the average flow rate. Based on this fact, intermittent turbulence may prevail in the flow field, whereby turbulence may first be initiated locally in the wave, even at relatively low average film Reynolds numbers (Re), and may extend further to the substrate film with increasing flow rate (Brauner & Moalem Maron 1988).

A first step to account for local turbulence in the flow field has been presented recently (Brauner 1987). Utilizing energy considerations, analytical expressions have been presented for the roll wave celerity and average film thickness in fully developed turbulent wavy film flow. It is the purpose of the present work to establish a comprehensive turbulent wave model, based on different physical mechanisms controlling the various zones along the waves, for intermediate Re, where turbulence may develop only at the wave core region and for fully turbulent wavy flow, where turbulence extends to the entire substrate film.

2. THE PHYSICAL MODEL

A schematic description of the physical phenomena associated with a typical large rolling wave, as viewed in a coordinate system moving with the wave velocity, is outlined in figure 1(a). A roll

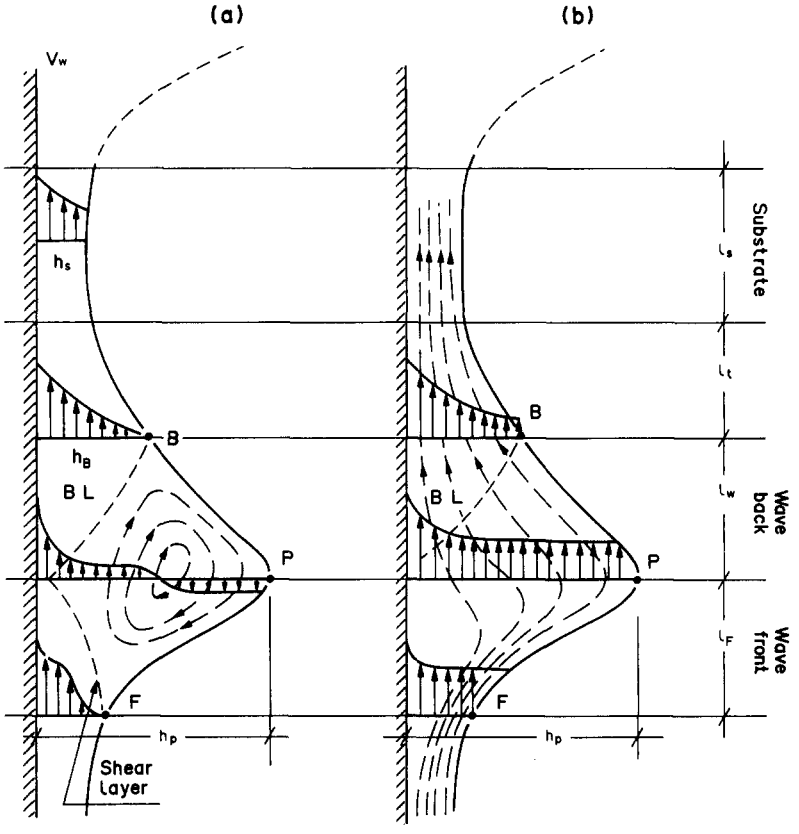

Figure 1. Schematic description of a wave in moving coordinates: (a) stagnation at B; (b) extremum (non-stagnation) at B.

wave is visualized as a lump of liquid travelling over a slow-moving thin substrate film. In moving coordinates the substrate entering the wave resembles a fast-moving wall jet entering the region of slower-moving liquid, and a shear layer can be expected to develop as shown in the diagram. Away from the wall, in the wave core, a large mixing eddy is formed. Simultaneous measurements of the local and instantaneous film thickness and mass transfer rates (Brauner & Moalem Maron 1982) or wall shear (Zabaras 1985) indicate that the near-wall region is characterized by a periodical process of distortion of the wall boundary-layer (BL) at the frontal region and its reestablishment at the wave back. In the moving coordinates system, which follows the wave motion, the solid wall is seen as drawn away from the liquid lump at the wave velocity, V_w. Thus, the BL is that which develops on continuous surface; it grows in the direction of the wall motion and terminates at point B, where the BL thickness becomes identical to the local film thickness h_B.

The above physical picture led Brauner & Moalem Maron (1983) to introduce the idea of a stagnation condition (in moving coordinates) at B. This idea has been recently explored analytically by Brauner *et al.* (1987c) to justify the existence of either stagnation or extremum conditions at the interface. It has been shown that the downstream interfacial velocity, v_i, attains either the wave velocity at both the wave back and front [stagnation in moving coordinates at points B and F as sketched in figure 1(a)] or it attains a maximum value at B with $v_{iB} = (v_i)_{max} < V_w$, followed by a minimum value at the front $v_{iF} = (v_i)_{min}$. The corresponding streamlines and velocity profiles $u(y)$, viewed in moving coordinates, for these two possible situations are sketched in figures 1(a,b). Note that $u(y) = v(y) - V_w$.

The presence of stagnation points is associated with a recirculating eddy (viewed in moving coordinates), highest downstream velocities at the peak region and a sharp change in velocities between the wave core and substrate ahead, which generates shear-layer conditions at the wave front [figure 1(a)]. The existence of extremum points along the free interface, however, corresponds to gradual changes in velocities within the wave and relatively low downstream velocities at the

wave peak region (Brauner *et al.* 1987c). The latter is schematically outlined in figure 1(b). A similar description of streamlines within the wave confinement (with no internal circulation) has been obtained numerically by Bach & Villadsen (1984) for low Re.

Whether point B is an extremum point or a stagnation point, it represents the boundary between the two regions of the wave trail. The first region is that of the substrate film, where the velocity distribution may reasonably be described by similarity profiles (scaled with reference to the local film thickness h) and the interfacial velocity monotonically decreases with the decrease in the local film thickness towards its final constant value, h_s. The second region is the wave back, which includes two subzones: the near-wall region where the velocity profiles are scaled relative to the local BL thickness, δ; and an outer region of near uniform velocity between δ and h.

The formulations of the continuity and momentum equations for the various wave zones for a fully turbulent or intermittent turbulent flow field are presented briefly below. The fully laminar model equations are listed in appendix A. The details of the derivations are given in Brauner (1988).

2.1. *Integral Continuity Relationships*

The integral continuity equations in a moving coordinates system applied at several specific locations along the wave read as follows:

$$h(V_w - V) \overset{[a]}{=} h_p(V_w - V_p) \overset{[b]}{=} h_B(V_w - V_B) \overset{[c]}{=} h_s(V_w - V_s) \overset{[d]}{=} \gamma, \qquad [1a\text{–}d]$$

where V is the local velocity averaged across the local film thickness h and γ is an apparent constant discharge rate of the fluid. The subscripts p, B and s stand for the peak, the location of the B plane and the substrate, respectively.

In a stationary coordinates system, the time average mass flow rate is equal to the mass feed rate, Γ, which yields (Brauner 1987):

$$\frac{\frac{\Gamma}{\rho} + \gamma}{F} = \int_0^{\lambda} h \, dl \qquad [2]$$

with

$$\lambda = \frac{V_w}{F} = l_F + l_w + l_t + l_s. \qquad [3]$$

Here F and λ are the wave frequency and wavelength, respectively; l_F, l_w and l_s are the lengths of the wave front, the wave back and the substrate film, respectively, and l_t is the substrate varying thickness region [see figures 1(a,b)].

Since the slope of the wave is $< 10\%$, even at its steepest location, the wave front and wave back shape are approximated by straight lines, and [2] is integrated to give a relation for the wave frequency in terms of the wave dimensions, whereby

$$F = \frac{2\left(\frac{\Gamma}{\rho} + \gamma - V_w h_s\right)}{\left[l_F\left(\frac{h_p}{h_s} - 1\right) + l_w\left(\frac{h_B}{h_s} + \frac{h_p}{h_s} - 2\right) + l_t\left(\frac{h_B}{h_s} - 1\right)\right]h_s} \qquad [4]$$

with

$$\frac{l_t}{l_w} = \frac{(h_B - h_s)}{(h_p - h_B)}. \qquad [5]$$

2.2. *Modelling the Shedding Rate, γ*

As has been noted above, point B defines the boundary between the wave back and the substrate region. At this point the interfacial velocity either attains its maximum value, where $V_{iB} = (v_i)_{max} < V_w$, or it attains the wave velocity with $v_{iB} = V_w < (v_i)_{max}$. In previous works, (Brauner & Moalem Maron 1983; Moalem Maron *et al.* 1985; Brauner *et al.* 1987c) it has been elucidated

that the inertia terms at point B are practically negligible and thus, the local film thickness can be evaluated by equating the local body and viscous forces. The existence of stagnation conditions at B provides an additional relationship in terms of the wave velocity, whereas in the case of extremum conditions at B, the solution proceeds in terms of an initially unspecified parameter, $\xi_0 = 1 - v_{iB}/V_w$. Thus, ξ_0 represents the deviation of the local interfacial velocity from the stagnation condition.

For sufficiently high local Re, turbulence may prevail in the wave back region. The velocity profile at point B is then assumed to obey a power-law of velocity distribution (Schlichting 1968), whereby

$$\frac{v}{V_w} = (1 - \xi_0)\left(\frac{y}{h_B}\right)^{1/n}. \qquad [6]$$

The corresponding local average velocity and local wall shear at B are given by (Schlichting 1968)

$$V_B = \frac{1}{h_B}\int_0^{h_B} v\, dy = \frac{n}{n+1}(1 - \xi_0)V_w \qquad [7]$$

and

$$\frac{\tau_{wB}}{\rho V_w^2} = S(n)\left(\frac{\nu}{h_B V_w}\right)^{2/(n+1)}(1 - \xi_0)^{2n/(n+1)}, \qquad [8]$$

where $S(n) = [1/C(n)]^{2n/(n+1)}$ and $C(n)$ is a coefficient determined by the power n, used in [6]; $C(n) = 8.74$ for $n = 7$.

It is to be noted that in spite of the fact that a power-law velocity characterizes in a strict sense only fully developed turbulent flows in pipes, it has been shown to be a useful approximation in other cases. The advantage of using such a profile is the possibility of obtaining closed analytic expressions, which make the theory mathematically amenable, albeit slightly inaccurate.

Equating the local body force with the local wall shear at point B, [8] yields an expression for h_B:

$$\frac{h_B}{h_{B_0}} = (1 - \xi_0)^{2n/(n+3)}, \qquad h_{B_0} = \left[\frac{S(n)^{(n+1)}\nu^2}{g^{(n+1)}} V_w^{2n}\right]^{1/(n+3)}; \qquad [9]$$

where h_{B_0} is the corresponding local film thickness in the case where point B is a stagnation point ($\xi_0 = 0$).

The shedding rate is obtained by applying [1a–d] at point B, with V_B and h_B, defined by [7] and [9], which then yields:

$$\gamma = \gamma_0 f(\xi_0), \qquad f(\xi_0) = (n\xi_0 + 1)(1 - \xi_0)^{2n/(n+3)}; \qquad [10]$$

and

$$\gamma_0 = \left[\frac{S(n)^{(n+1)}\nu^2}{(n+1)g^{(n+1)}} V_w^{3(n+1)}\right]^{1/(n+3)}. \qquad [11]$$

Again, γ_0 is the corresponding shedding rate in the case where point B is a stagnation point ($\xi_0 = 0$). The shedding rate, γ, increases with increasing ξ_0, and with $n = 7$ it attains a maximum value for $\xi_0 = 1/3$. As is shown below (section 2.5), the condition of maximum shedding rate determines the limit beyond which no physical solution exists for the wave pattern.

2.3. The Wave Back Region

The back of the wave is designated as the region between the wave peak and plane B. At this region a wall BL is reestablished. Its growth is assumed to start under the wave peak and to terminate at plane B, where the local BL thickness becomes identical to the local film thickness. In the moving coordinates system, which follows the wave motion, the solid wall is seen as drawn away from the wave back, and, thus, the BL is that which develops on a continuous moving surface. Applying BL theory via the integral approach provides expressions for the length of the wave back,

l_w, and the variation of the wall shear at this region (based on the power-law velocity profile across the BL):

$$l_w = \frac{2}{(n+2)(n+3)} F(\Delta_0, \xi_0) \frac{V_w^2}{g}, \qquad [12]$$

where

$$F(\Delta_0, \xi_0) = \left[\left(\frac{h_B}{h_{B_0}}\right)^{(n+3)/(n+1)} - \Delta_0^{(n+3)/(n+1)}\right] \frac{\{\xi_0[n(1-\xi_0)-2]+2\}}{2(1-\xi_0)^{2n/(n+1)}} \qquad [13]$$

and $\Delta_0 = \delta_0/h_{B_0}$ denotes the residual (initial) BL thickness under the wave peak.

The average wall shear stress at the wave back region, $\bar{\tau}_w$, is expressed in terms of a wall shear parameter, K_w, defined by

$$K_w = \frac{\bar{\tau}_w}{\tau_{w_B}} = \frac{1}{\rho g h_B L_w} \int_0^{L_w} \tau_w(\Delta)\, dX = \frac{(n+3)}{(n+1)} \frac{\left[\frac{h_B}{h_{B_0}} - \Delta_0\right]\left(\frac{h_B}{h_{B_0}}\right)^{2/(n+1)}}{\left[\left(\frac{h_B}{h_{B_0}}\right)^{(n+3)/(n+1)} - \Delta_0^{(n+3)/(n+1)}\right]}; \qquad [14]$$

K_w is the ratio between the shear stress averaged over the wave back, $L_w = l_w/h_{B_0}$, and the local wall shear stress at plane B. As indicated in [14], the possible range of K_w is determined by the variation of the residual thickness of the BL, Δ_0. For $\Delta_0 \to 0$, K_w attains its maximum value [for $\xi_0 = 0$ and $n = 7$, $K_w = (K_w)_{max} = 1.25$]. A lower bound for K_w results assuming the shear-layer formed at the front has almost no effect on the near-wall region, so that $\Delta_0 \simeq h_s/h_{B_0}$ under the peak of the wave.

The expressions derived for l_w and τ_w are utilized in a global momentum balance (in a moving coordinates system) performed over the wave back which yields a quadratic equation in h_p/h_B:

$$A\left(\frac{h_p}{h_B}\right)^2 + B\left(\frac{h_p}{h_B}\right) + C = 0 \qquad [15a]$$

with

$$A = 1,$$

$$B = -2K_w + 1 + \frac{(n+2)(n+3)f^2(\xi_0)}{(n+1)^2 F(\Delta_0, \xi_0)(1-\xi_0)^{4n/(n+3)}} \qquad [15b]$$

$$C = -\frac{(n+2)(n+3)f^2(\xi_0)}{(n+1)^2 F(\Delta_0, \xi_0)(1-\xi_0)^{4n/(n+3)}}.$$

2.4. The Wave Front Region

An integral momentum balance on the wave front (in a coordinates system moving with the wave velocity) provides an equation for the length of the wave front in terms of the other wave variables:

$$l_F = \frac{2\gamma^2}{g h_s h_p} \frac{\left(\frac{h_p}{h_s} - 1\right)}{\left(1 + \frac{h_p}{h_s} - 2K_F\right)}; \qquad K_F = \frac{\bar{\tau}_{w_F}}{\rho g h_s}. \qquad [16]$$

Based on experimental observations of wall shear relaxation in the wave front, $\tau_{w_F} \simeq 0$ may be comfortably assumed (Moalem Maron *et al.* 1985).

2.5. The Substrate Film Region

The substrate is visualized as the region beyond plane B, where deceleration of the film takes place and a constant film thickness, h_s, is established.

It has been shown that the fraction of liquid flowing in the substrate (based on the laminar film) may range between 4–20% of the total rate (Brauner & Moalem 1983; Moalem Maron *et al.* 1985). Thus, the major part of the flow rate is carried downstream by the liquid lumps—the rolling large

waves. The transition to turbulence is controlled by the local instantaneous Re, which is expected to attain a transitional value first in the wave back region. Thus, intermittent turbulence may be initiated in the flow field even at relatively low overall (feed) Re, with turbulence prevailing in the wave back region, while the thin substrate film is laminar. However, at high liquid flow rates, turbulence may develop not only in the wave back region, where it is first initiated, but also in the wave trail region, and may further extend to the substrate film region. Therefore, appropriate modelling of the substrate ought to be adopted in the integrated wave model.

Laminate substrate–turbulent wave back, L–T

For the laminar substrate film, the velocity distribution in the film is parabolic and the average local velocity, V_s, is given by

$$V_s = \frac{1}{3}\frac{\rho g}{\mu} h_s^2. \qquad [17]$$

Utilizing [1a–d], [7], [9] and [17] results in a cubic equation for (h_s/h_B):

$$\left(\frac{h_s}{h_B}\right)^3 - \frac{3}{(1-\xi_0)S(n)^{2(n+1)/(n+3)}}\left[\frac{gv}{(1-\xi_0)^3 V_w^3}\right]^{(n-1)/(n+3)}\left[\frac{h_s}{h_B} - \frac{(n\xi_0+1)}{(n+1)}\right] = 0. \qquad [18]$$

As is indicated by [18], the solution obtained for (h_s/h_B) is dependent on the wave velocity.

Turbulent substrate–turbulent wave back, T–T

In this case, the nth power turbulent velocity profile is assumed for the substrate film, with the local average velocity and wall shear stress given by

$$V_s = v_{is}\frac{n}{n+1} \qquad [19]$$

and

$$\tau_{ws} = S(n)\rho v_{is}^2\left(\frac{v}{h_s v_{is}}\right)^{n/(n+1)}. \qquad [20]$$

In the constant substrate film region, gravity is balanced by the wall shear, and thus an expression for V_s is derived:

$$V_s = \frac{n}{n+1}\left[\frac{g^{(n+1)}}{S(n)^{(n+1)}v^2} h_s^{(n+3)}\right]^{1/2n}. \qquad [21]$$

Substituting [7], [9] and [21] into [1a–d] yields an equation for (h_s/h_b), which reads as follows:

$$\frac{n(1-\xi_0)}{(n+1)}\left(\frac{h_s}{h_B}\right)^{3(n+1)/2n} - \frac{h_s}{h_B} + \frac{(n\xi_0+1)}{(n+1)} = 0. \qquad [22]$$

Note that the solution obtained for h_s/h_B in this case is independent of the wave velocity. For instance, for $n = 7$ and $\xi_0 = 0$, $h_s/h_B = 0.165$. For $\xi_0 = 1/3$, which corresponds to γ_{max} (by [10] and [11]), $h_s/h_B = 1$. Thus, the range of ξ_0, which yields physical solution for h_s, is limited to $0 \leqslant \xi_0 \leqslant 1/3$.

2.6. Prediction of the Wave Velocity

The wave frequency and wave velocity are continuously varying during the development of the wavy flow. At the inception region, high frequency, dense ripples with relatively low translational speed are initiated (Brauner & Moalem Maron 1982).

With the acceleration process taking place downstream, overlapping occurs and the frequency decreases, while the wave velocity, wavelength and amplitude increase (Brauner & Moalem Maron 1982; Webb & Hewitt 1975; Takahama & Kato 1980). Far downstream of the inception region, a fully developed wavy flow is established. The ultimate frequency and the corresponding wave velocity are inherent properties of the fully developed wavy pattern. The approach towards the fully developed pattern depends on various operating conditions, such as liquid flow rate, surface inclination and the particular mode of the liquid feed distribution.

For a given set of operating conditions the wave velocity at the upstream inception region and the asymptotic wave velocity downstream may be regarded as lower and upper bounds for the probable wave velocity range. These are predicted as follows.

Inception wave velocity—lower bound

The wave velocity of the high frequency, dense waves, at the wave inception region is evaluated by setting the length of the constant thickness substrate region identical to zero. Equation [3] then reads:

$$V_{w_{min}} = F(l_F + l_w + l_t); \qquad l_s = 0. \tag{23}$$

As the total number of (unknown) wave variables is now reduced ($l_s = 0$), incorporation of [23] in the model equations provides an evaluation of the inception wave velocity.

Equilibrium wave velocity—upper bound

The ultimate wave velocity in the fully developed wavy flow region, corresponds to an asymptotic equilibrium state, whereby the average dissipated energy in the liquid film during a wave period is balanced by the corresponding average work done by gravity (Brauner 1987). The equilibrium wave pattern is associated with a minimum value for the average film thickness $\bar{h}$, which by [2] and [3] reads:

$$\bar{h} = \frac{1}{\lambda}\int_0^{\lambda} h \, dl = \frac{1}{V_w}\left(\frac{\Gamma}{\rho} + \gamma\right), \tag{24}$$

where, γ is given in either [10] and [11] (turbulent model) or in [A.3] (laminar model, appendix A) as a function of the wave velocity and ξ_0. The conditions for which $\bar{h}$ attains a minimum value has been derived by Brauner & Moalem Maron (1983) for laminar wavy flow and by Brauner (1987) for turbulent wavy flow, assuming the stagnation condition at B, $\xi_0 = 0$. These conditions are rederived below for $\xi_0 \geqslant 0$ (the corresponding laminar equations are given in appendix A).

The shedding rate γ, given in [10] and [11] reads:

$$\gamma = Af(\xi_0)V_w^{m+1}, \tag{25}$$

where

$$A = \frac{1}{n+1}\left[\frac{S(n)^{(n+1)}\nu^2}{g^{n+1}}\right]^{1/(n+3)}; \qquad m = \frac{2n}{n+3}; \quad \text{turbulent.} \tag{26}$$

Since all the wave variables are related to the wave velocity (through the model equations), ξ_0 is assumed to be dependent on the wave celerity. An extremum value of $\bar{h}$ exists providing $d\bar{h}/dV_w = 0$. Substituting [25] and [26] into [24], this condition results in an algebraic equation for the equilibrium wave celerity, C:

$$\left\{\left[\frac{(n+1)(n+3)}{8n}\right]^{(n+3)}\left[\frac{48}{S(n)}\right]^{(n+1)}\mathrm{Re}^{(1-n)}\right\}^{1/3(n+1)} = C\left\{f(\xi_0)\left[1 + \frac{(n+1)}{2}C\frac{(1-3\xi_0)}{(1-\xi_0)(1+n\xi_0)}\frac{d\xi_0}{dC}\right]\right\}^{(n+3)/3(n+1)}. \tag{27}$$

Here, Re is the feed Reynolds number ($= 4\Gamma/\mu$); C is the dimensionless wave celerity, $C = V_w/V_N$; and V_N is the average Nusselt's velocity, $V_N = (1/48\nu g\,\mathrm{Re}^2)^{1/3}$. For any specified power-law used and $\xi_0(C)$, [27] can be solved for $C = C_{eq}$. For instance, for $n = 7$, $S(n) = 0.0225$ and $\xi_0 = \text{const}$, [27] reads:

$$C_{eq} = 14.93(1-\xi_0)^{-7/12}(1+7\xi_0)^{-5/12}\mathrm{Re}^{-1/4}. \tag{28}$$

Equation [28] for $\xi_0 = 0$ (stagnation at B) yields $C_{eq} = 14.93\mathrm{Re}^{-1/4}$, as derived previously by Brauner (1987).

2.7. Solution Procedure

The relationships presented above for each of the wave regions include 13 unknowns: (l_F, h_p, V_p), (l_w, h_B, V_B), (l_t, l_s, h_s, V_s) (V_w, F, γ).

A functional relationship $\xi_0 = f(C)$ is to be prescribed (see below), which provides ξ_0 in the limits where a physical solution exists. The mathematical formulations in sections 2.1–2.5 provide 12 independent relationships given in: [16], [15a], [1b]; [12], [9], [7]; [5], [3], [22], [21]; and [4], [10]. For the intermittent turbulent flow field (laminar substrate–turbulent wave back, L–T [21] and [22] are replaced by [17] and [18], while the fully laminar wavy model is calculated by replacing [7], [9], [10], [12], [21] and [22] by the corresponding equations given in appendix A. Note that, for the turbulent regime, the 7th power-law is used [$n = 7$, $S(n) = 0.0225$].

Thus, selection of one of the variables is sufficient to determine the others. That degree of freedom is attributed to the wave velocity, which is convenient to determine experimentally, and thus, the applicability of the model is extended to quasi-steady wave structure in the developing region.

The prediction of the wave velocity in section 2.6, in the wave inception region [23] or in the fully developed region [27] (or [A.9] in appendix A), provides an additional required relationship for the closed-form solution.

3. RESULTS AND DISCUSSION

The network of equations presented above represents a mathematical formulation of the physical mechanisms thought to take place in each of the wave zones. For a given set of operating conditions, all the wave variables are determined by the wave celerity, $C = V_w/V_N$. The computation also requires a prescription of the functional relation $\xi_0(C)$, which as yet is of an unknown nature. A parametric analysis is used below to show the impact of ξ_0 on the wave variables, while comparison with the experimental data provides an insight into the possible applicability of the relation $\xi_0(C)$.

As has been pointed out already, the observed wave velocity in the developing region is expected to be bounded by the wave velocity at the upstream inception region (lower bound, [23]) and the asymptotic equilibrium wave velocity downstream (upper bound, [27] or [A.9]). These predicted bounds are presented in figure 2 for a wide range of Re. Tap water physical properties have been used, and the results are compared with experimental data obtained by Chu (1973), Webb & Hewitt (1975) and Zabaras (1985).

In the fully laminar wavy flow regime the predicted bounds on the wave celerity are both independent of Re. The equilibrium wave celerity [A.9] decreases with increasing ξ_0 from its maximum value $C_{eq}(\xi_0 = 0) = 3.78$. On the other hand, the inception wave celerity increases with

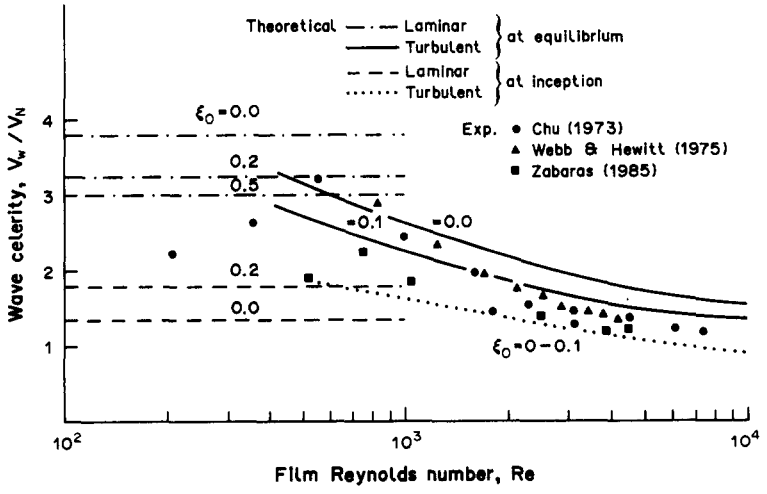

Figure 2. Predicted bounds on wave celerity—comparison with experimental data.

ξ_0 from its minimum value $C_i(\xi = 0) = 1.35$. Thus, the possible range of the predicted wave celerities diminishes with increasing ξ_0. For $\xi_0 \to 0.5$, which is the upper bound on the possible physical range of ξ_0 in the laminar regime, $C_{eq} \to 3.0$. This result is identical to those obtained in previous studies, which represent different theoretical approaches. For instance, stability analyses (assuming infinitesimal perturbations on the smooth laminar solution) and kinematic wave theory (Wallis 1969) both predict an upper limit of 3.0 for the wave celerity (Brauner *et al.* 1987a). Thus, the limit of $\xi_0 = 0.5$ may relate to a laminar rippled interface.

In the case where turbulence prevails at the wave back, the model predicts that both the equilibrium and inception wave celerities decrease with increasing Re. Both may go below the value of $C = 1.5$, predicted by stability analyses of a laminar film for high Re (Brauner *et al.* 1987a). As in the laminar case, the range between predicted bounds diminishes with increasing ξ_0. In the limit of $\xi_0 = 1/3$, which is the upper bound on the possible physical range of ξ_0 in the turbulent wave model, C_{eq} approaches the celerity obtained for kinematic waves in turbulent film flow, as derived in appendix B.

Inspection of figure 2 indicates that the experimental data taken at finite downstream locations is reasonably confined between the bounds predicted with $\xi_0 = 0$–0.2. Moreover, the turbulent model predictions are in reasonable agreement with the experiments already at Re $\approx$ 600–800, while the laminar model predictions are inadequate at Re > 1000. Thus, it can be speculated at this point that the transition to turbulent wavy flow, initiated by local turbulence at the wave back, takes place at Re > 600.

The evaluation of the model with respect to experimental data for various other wave characteristics (such as wave amplitude and frequency, substrate thickness) obtained in the developing region, is proceeded by utilizing the corresponding experimental data of the wave velocity, rather than the predicted bounds.

A comparison between the predicted and experimental average substrate thickness (Chu 1973), is presented in figures 3(a–d). The predicted substrate thickness is obtained by [18], [22] and [A.7], depending on whether laminar or turbulence prevail at the wave back and substrate regions. The values predicted through the laminar–laminar model (L–L), [A.7], are presented in figure 3(a); those which are obtained at the intermediate laminar–turbulent case (L–T), whereby the wave back is turbulent while the substrate film remains laminar, [18], are presented in figure 3(b); the fully turbulent model results (T–T), [22], are presented in figure 3(c). As is indicated in the figures,

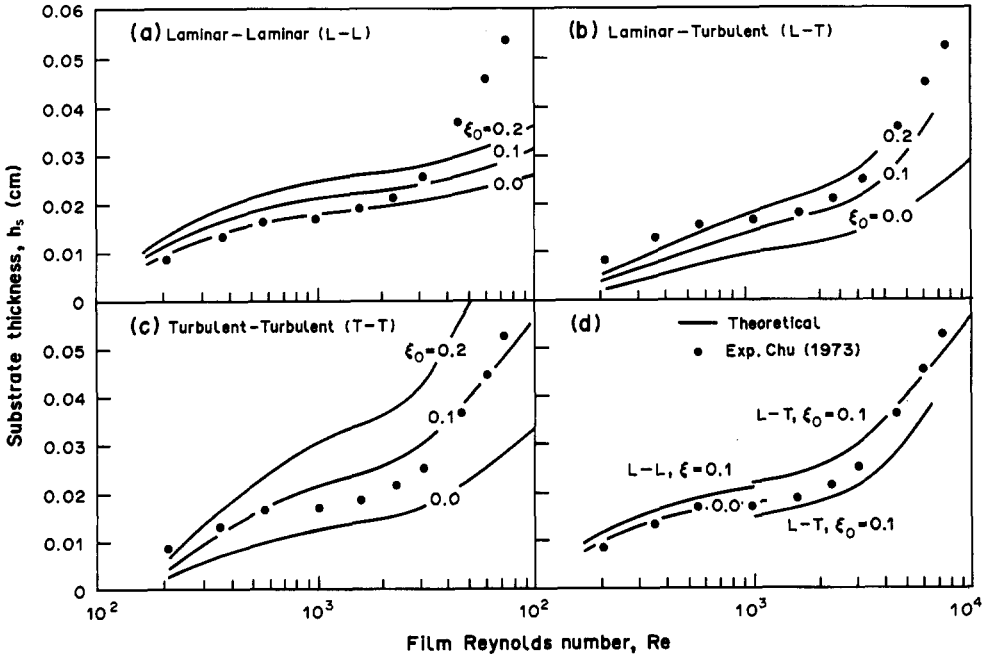

Figure 3. Substrate film thickness—comparison of theory with experimental data.

increasing ξ_0 (non-stagnation condition), effects an increase in the predicted substrate thickness. Inspection of figure 3(a) reveals that the moderate increase in the measured substrate thickness with Re for Re < 1000 is well-predicted by the L–L model. For higher Re, the rather steep increase in the substrate thickness with Re is well-predicted either by the L–T model in the intermediate Re range or by the T–T model in the high Re range, both accounting for the role of turbulence at the wave back [figures 3(b,c)]. Still, it is difficult to judge whether turbulence has been extended to the substrate film, since the two solutions differ by <20%. It is to be noted, however, that for sufficiently high Re, no physical solution is obtained for the L–T model. For instance, with $\xi_0 = 0$ the L–T model is limited to Re < 10,000, and the limit decreases with increasing ξ_0; $Re_{max} \simeq 4000$ for $\xi_0 = 0.2$. This implies that in the high Re range, turbulence in the stagnation region extends to the substrate region and only fully turbulent wavy situations may exist. The three models are combined in figure 3(d), where transitions from L–L to L–T and from L–T to T–T are suggested in view of the data. As is shown in figure 3(d), the value of $\xi_0 \simeq 0.1$ reasonably predicts the substrate thickness for a wide range of Re [based also on recent findings in the laminar regime (Brauner *et al.* 1987b)].

The predicted substrate Reynolds number, $Re_s = 4h_s V_s/\nu$, is presented in figure 4. Consistent with the physical model, the Re_s is about 5–20% of Re as the major part of the feed rate is carried downstream by the wave lumps. Indeed, for Re < 1000, as suggested in figure 2, $Re_s < 100$, by figure 4, and thus the L–L model is applicable. For Re > 1000, the Re_s predicted by the L–T model sharply increases with increasing Re, approaching the values predicted by the T–T model. For instance, Re > 6000 corresponds to $Re_s > 1000$ according to both the L–T and T–T models. Hence, the application of the fully turbulent wavy model in this region is justified.

Figure 5 compares the calculated values of the wave amplitude with experimental data obtained by Chu (1973) and Zabaras (1985). The experimental data are shown along with the theoretical curve of the smooth Nusselt film thickness, h_N. It seems that Chu's data at the lowest laminar flow rates are in error, since h_p is expected to exceed h_N. The theoretical curves correspond to a value of $\Delta_0 = 0$ and thus $K_w = (K_w)_{max}$ (by [14] or [A.6]) and $h_p = (h_p)_{max}$. Note that, in this case the solution for the wave height, h_p, is unaffected by the substrate thickness value, and the L–T and T–T models yield identical values for h_p. As is shown in figure 5, again the measured values are reasonably predicted by the laminar wave model for Re < 1000 ($\xi_0 = 0$–0.2), while for Re > 1000 the increase in the wave height with Re is well-predicted by the turbulent wave models. The

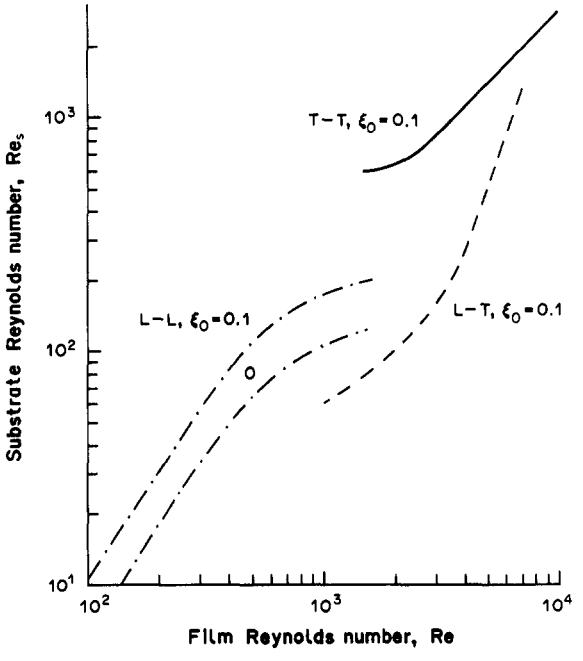

Figure 4. Substrate film Reynolds number (Re_s) as function of feed Reynolds number (Re).

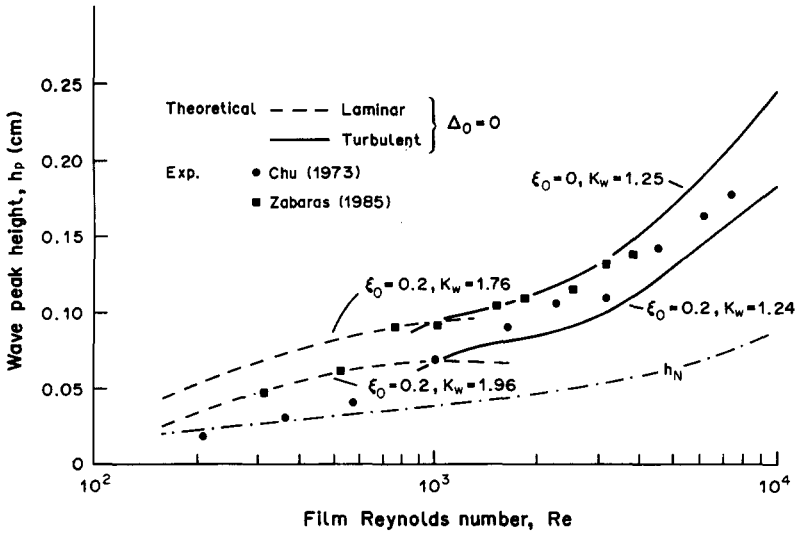

Figure 5. Wave peak height—comparison of theory with experimental data.

predicted values decrease with increasing ξ_0, and the value of $\xi_0 \geqslant 0.2$ already underpredicts the observed values. The increase in h_p with higher velocities in the peak region, on the one hand, and the decrease of h_s with reduced velocities at the substrate, on the other, with decreasing ξ_0, represents, in fact, the process of roll wave development from an initially rippled interface. Variability of ξ_0 between successive waves may account for the observed random nature of the wave structure.

The effect of Δ_0 on the predicted wave height is explored in figure 6, where predicted values for h_p for $0 \leqslant \Delta_0 \leqslant \Delta_{0_{max}} = h_s/h_{B_0}$ and $\xi_0 = 0.1$ are compared with the experimental data. The corresponding value for K_w is given by [14] or [A.6]. As is shown in the figure, increasing Δ_0 results in a smaller wave height both in the laminar and turbulent models. The predicted values through the L–T and T–T models with $\Delta_{0_{max}}$ are almost identical. Again, the value of $\xi_0 \simeq 0.1$ with $0 \leqslant \delta_0 \leqslant h_s$ reasonably predicts the wave height over the whole range of Re.

A comparison between the predicted wave frequency and the experimental data is given in figure 7. The theoretical values are in reasonable agreement with the trends of the experimental data. It is to be noted that experimental wave data obtained for short flow surfaces exhibits higher wave frequencies, which corresponds to underdeveloped waves. In general, the turbulent model predicts higher frequencies in the high Re range.

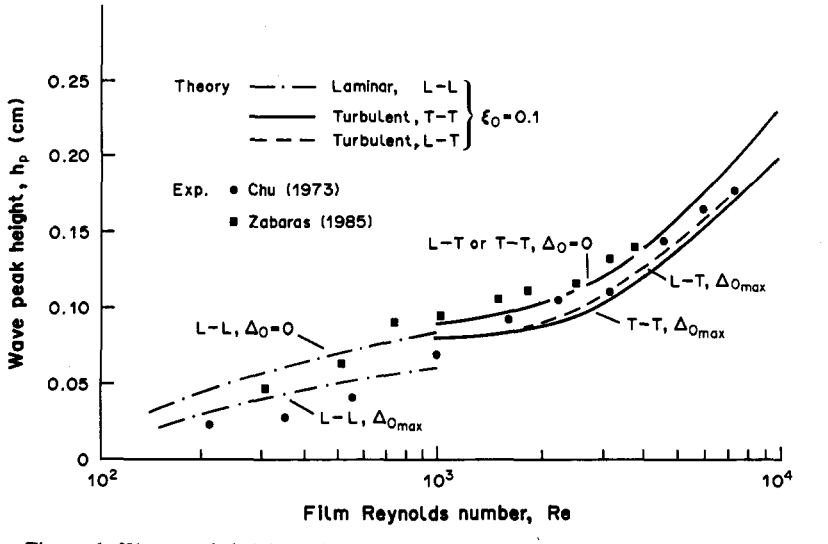

Figure 6. Wave peak height—effect of the residual boundary layer thickness, δ_0.

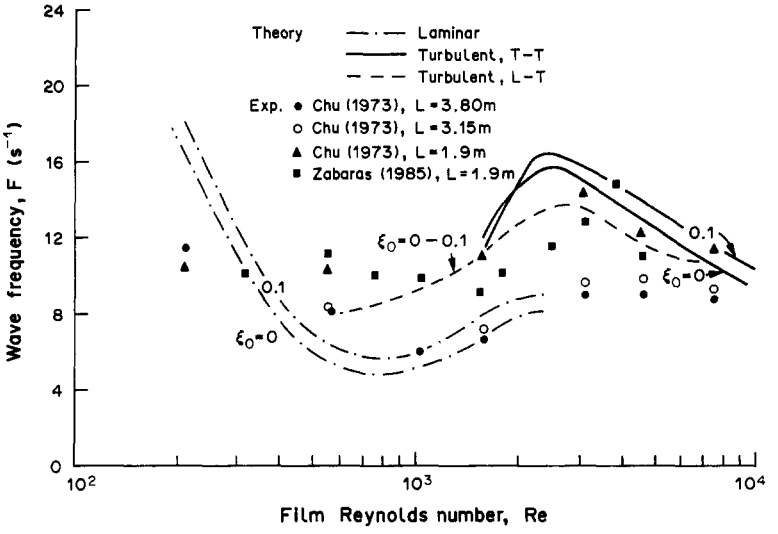

Figure 7. Wave frequency—comparison of theory with experimental data.

In view of the reasonable agreement shown so far between experimental and theoretical results with $\xi_0 \simeq 0.1$, it is suggested herein that the interfacial condition at point B is close to stagnation over a wide range of Re. However, the applicability of $\xi_0 \simeq 0.1$ does not necessarily indicate that the flow pattern within the wave confinement corresponds to the non-stagnation condition [figure 1(b)]. One may assume that stagnation at B exists, while introducing a non-zero value for ξ_0 compensates for the neglect of inertia forces at B. As has been noted by Brauner *et al.* (1987c), the existence of the small bow waves ahead of the large rolling wave, may indicate that the wave pattern corresponds to stagnation conditions since the appearance of a bow wave train evolves from a sharp change in velocities between the substrate film and the wave core [figure 1(a)]. Thus, it is also likely that $\xi_0 \neq 0$ is to be considered as a way to account for the effects of inertia around the stagnation area. In fact, recent numerical simulations on the flow pattern inside a rolling wave (Moalem Maron & Hewitt 1988; Moalem Maron *et al.*, 1989; Wasden & Dukler 1988) have verified the existence of a recirculating region and the associated stagnation points at the front and rear of the wave [as sketched in figure 1(a)].

The discussion proceeds at this point, speculating on the required functional relation for ξ_0. It is expected that ξ_0 relates to the various wave characteristics and to the flow regime. However, since the wave characteristics are determined by the wave velocity, it turns out that $\xi_0 = f(C)$. The simplest functional relation that can be assumed is a linear one, whereby $\xi_0 = aC + b$. The parameters a and b are chosen to yield the best agreement with the data. Figure 8(a) presents the equilibrium wave celerity (upper bound) predicted with $\xi_0 = 0.05C$, [27] or [A.9]. The corresponding values which result for ξ_0 are presented in figure 8(b). Reasonable agreement between the theoretical predictions (via the turbulent wave model) and the experiments is observed for the wave celerity for Re > 1000. Also the predicted values of ξ_0 are in reasonable agreement with the values used for the demonstrations in figures 3–7. Incooperation of $\xi_0 = 0.05C$ in the laminar wave model [A.9], predicts a value of $C = 2.86$ and a corresponding value of $\xi_0 = 0.145$, both independent of Re.

Although the above results are in the range of the experimental data, a more sophisticated relation for $\xi_0 = f(C, \mathrm{Re})$, is probably required in order to predict the variation of the wave celerity with Re. Moreover, at low Re, ξ_0 may also depend on the capillary number, $C_a = \mu V_w/\sigma$ (Brauner 1987).

4. SUMMARY AND CONCLUDING REMARKS

Turbulent wavy flow models for intermediate and high Re are presented. The analytical development considers both stagnation or non-stagnation conditions at the wave back interface.

Comparison with experiments suggests that the wavy flow field is laminar up to Re $\simeq$ 1000. At

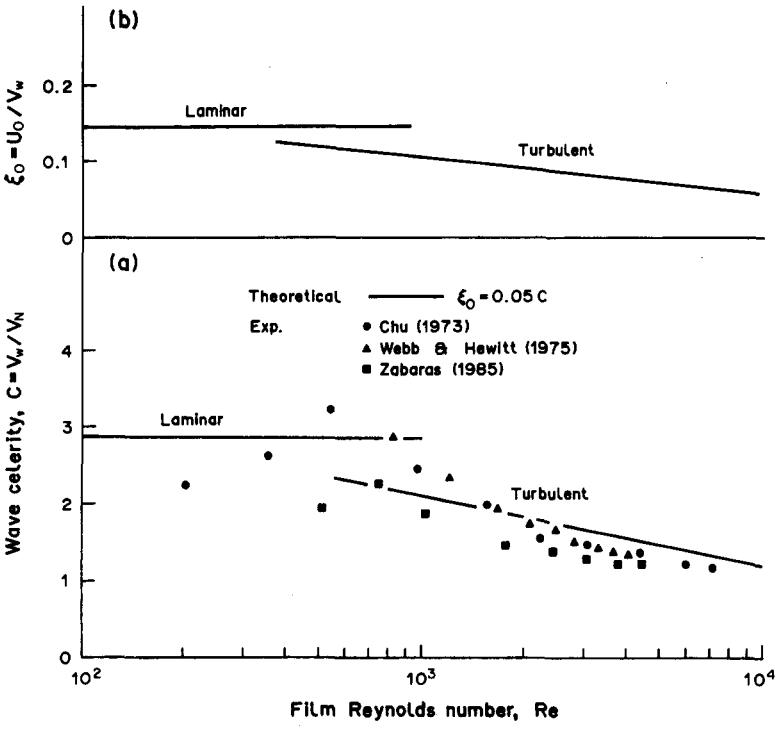

Figure 8. Equilibrium wave celerity—effect of the variable ξ_0.

intermediate Re ($1000 < \mathrm{Re} < 4000$) turbulence is initiated in the wave core region, while the substrate film remains laminar. In this region, intermittent turbulence is thus expected in the flow field. For higher Re, turbulence extends to the wave trail and substrate film, resulting in a fully turbulent way flow field.

The results point out that the condition in the wave back for a developed wave pattern is close to stagnation over a wide range of Re. The deviation from the stagnation condition obtained in the turbulent model is in the range of the expected velocity fluctuations in the flow field. The recirculating eddy (visualized in the wave core, in moving coordinates) may thus be considered as part of the turbulent field. Its main role lies in triggering the initiation of turbulence.

Acknowledgement—The author wishes to express her gratitude to Professor David Moalem Maron for many useful and illuminating discussions.

REFERENCES

BACH, P. & VILLADSEN, J. 1984 Simulations of the vertical flow of a thin wavy film using finite-element method. *Int. J. Heat Mass Transfer* **27**, 815–827.

BRAUNER, N. 1987 Roll wave celerity and average film thickness in turbulent wavy film flow. *Chem. Engng Sci.* **42**, 265–273.

BRAUNER, N. 1988 Modelling of wavy flow in turbulent free falling films. Report, Dept of Fluid Mechanics and Heat Transfer, Tel-Aviv Univ. Israel.

BRAUNER, N. & MOALEM MARON, D. 1982 Characteristics of inclined thin films waviness and the associated mass transfer. *Int. J. Heat Transfer* **25**, 99–110.

BRAUNER, N. & MOALEM MARON, D. 1983 Modelling of wavy flow in inclined thin films. *Chem. Engng Sci.* **38**, 775–788.

BRAUNER, N., & MOALEM MARON, D. 1988 Turbulent withdrawal: application to wavy flow modelling. *Chem. Engng J.* **37**, 1–10.

BRAUNER, N., MOALEM MARON, D. & DUKLER, A. E. 1985 Modelling of wavy flow in inclined thin films in the presence of interfacial shear. *Chem. Engng Sci.* **40**, 923–937.

BRAUNER, N., MOALEM MARON, D. & ZIJL, W. 1987a Interfacial collocation equations of thin liquid film: stability analysis. *Chem. Engng Sci.* **42,** 2025–2036.

BRAUNER, N., MOALEM MARON, D., ZABARAS, G. & DUKLER, A. E. 1987b Interfacial structure of thin falling films: piecewise modelling of waves with counter shear. *Chem. Engng Commun.* **58,** 245–272.

BRAUNER, N., MOALEM MARON, D. & TOOVEY, I. 1987c Characterization of the interfacial velocity in wavy thin films. *Int. Commun. Heat Mass Transfer* **14,** 293–302.

CHU, K. J. 1973 Statistical characterization and modelling of wavy liquid films in vertical two-phase flow. Ph.D. Thesis, Univ. of Houston, Tex.

CHU, K. J. & DUKLER, A. E. 1975 Statistical characteristics of thin films: III. Structure of the large waves and their resistance to gas flow. *AIChE Jl* **21,** 583–593.

MOALEM MARON, D. & HEWITT, J. 1988 Characterization of flow pattern in wavy thin film flow. Report, AERE Harwell, U.K.

MOALEM MARON, D., BRAUNER, N. & DUKLER, A. E. 1985 The interfacial structure of thin falling films: piecewise modelling of the waves. *PhysicoChem. Hydrodynam.* **6,** 87–113.

MOALEM MARON, D., BRAUNER, N. & HEWITT, J. 1989 Flow patterns in wavy thin films: numerical simulation. *Int. Commun. Heat Mass Transfer*. Submitted.

SCHLICHTING, H. 1968 *Boundary Layer Theory*, p. 566. McGraw-Hill, New York.

TAKAHAMA, H. & KATO, S. 1980 Longitudinal flow characteristics of vertically falling liquid films without co-current gas flow. *Int. J. Multiphase Flow* **6,** 203–215.

WALLIS, G. B. 1969 *One-dimensional Two-phase Flow*. McGraw-Hill, New York.

WASDEN, F. K. & DUKLER, A. E. 1988 Numerical investigation of large wave interactions on free falling films. Presented at *2nd Int. Symp. Two-phase Annular and Dispersed Flows*, Oxford, U.K.

WEBB, D. R. & HEWITT, G. F. 1975 Downwards co-current annular flow. *Int. J. Multiphase Flow* **2,** 35–49.

ZABARAS, G. J. 1985 Studies of vertical gas liquid flows. Ph.D. Thesis, Univ. of Houston, Tex.

APPENDIX A

Model Equations for Fully Laminar Wavy Film Flow

The shedding rate, γ

Following the derivation outlined in section 2.2, the corresponding equations obtained for laminar regime at B (which replace [7], [9] and [10]) are:

$$\frac{V_B}{V_w} = \frac{2}{3}(1-\xi_0), \tag{A.1}$$

$$h_B = \left(\frac{2\mu V_w}{\rho g}\right)^{1/2}(1-\xi_0)^{1/2} \tag{A.2}$$

and

$$\gamma = \frac{V_w}{3}\left(\frac{2\mu V_w}{\rho g}\right)^{1/2}(1-\xi_0)^{1/2}(1+2\xi_0) = \gamma_0 f(\xi_0), \tag{A.3}$$

with $\gamma(\xi_0 = 0.5) = \gamma_{max}$ in the laminar case.

The wave back region

The length of the wave back and the corresponding wall shear stress, derived based on laminar BL recovery (Brauner *et al.* 1987b), are given by

$$L_w = \frac{l_w}{h_{B_0}} = F(\Delta_0, \xi_0)\frac{V_w^2}{g h_{B_0}}, \tag{A.4}$$

where

$$F(\Delta_0, \xi_0) = \left[\frac{3}{100} - \frac{17}{3150}(1-\xi_0)\right][1-\xi_0]\left[1 - \frac{\Delta_0^2}{(1-\xi_0)}\right] - \frac{(1-\xi_0)^2}{1512}\left[1 - \frac{\Delta_0^4}{(1-\xi_0)^2}\right] + \frac{2}{125}(5+4\xi_0)(1-\xi_0)\ln\left[6 - 5\frac{\Delta_0^2}{(1-\xi_0)}\right] \tag{A.5}$$

and

$$K_w = \frac{1}{\frac{h_B}{h_{B_0}} L_w}\left\{\left[\frac{3}{250}+\frac{83}{7875}(1-\xi_0)\right]\left[1-\frac{\Delta_0}{(1-\xi_0)^{1/2}}\right][1-\xi_0]\right.$$
$$+\frac{1}{6}\left[\frac{1}{50}-\frac{98}{11{,}025}(1-\xi_0)\right](1-\xi_0)\left[1-\frac{\Delta_0^3}{(1-\xi_0)^{3/2}}\right]-\frac{1}{11{,}340}(1-\xi_0)^2\left[1-\frac{\Delta_0^5}{(1-\xi_0)^{5/2}}\right]$$
$$\left.+\frac{108}{125}\left(\frac{6}{5}\right)^{1/2}(1-\xi_0)\left[\frac{1}{6}-\frac{2}{27}(1-\xi_0)\right]\ln\left[21.95\frac{[1.095(1-\xi_0)^{1/2}-\Delta_0]}{[1.095(1-\xi_0)^{1/2}+\Delta_0]}\right]\right\}. \qquad [A.6]$$

For $\xi_0 = 0$ and $\Delta_0 = 0$ $K_w = (K_w)_{max} = 1.92$. Note that in laminar wave modelling [A.4] and [A.6] replace [12]–[14]. Also, in [15b] $C = -2/9f^2(\xi_0)F^{-1}(\Delta_0, \xi_0)(1-\xi_0)^{-1}$ and $B = 1 - 2K_w - C$.

The substrate film region, L–L

$$\left(\frac{h_s}{h_B}\right)^3 - \frac{3}{2}\frac{1}{(1-\xi_0)}\left(\frac{h_s}{h_B}\right) - 1 + \frac{3}{2}\frac{1}{(1-\xi_0)} = 0. \qquad [A.7]$$

Equation [A.7] is the substitute for [40], derived for fully turbulent way flow. The solution for h_s/h_B is independent of the wave velocity. For instance, for $\xi_0 = 0$ $h_s/h_B = 0.366$, and by [A.2] $h_s = 0.52(\mu V_w/\rho g)^{1/2}$. For $\xi_0 = 0.5$, which corresponds to maximum shedding rate, [A.7] yields $h_s/h_B = 1$. Thus, the physical range for ξ_0 in the fully laminar case is $0 \leqslant \xi_0 \leqslant 0.5$.

Prediction of the equilibrium velocity—upper bound

In the case where the laminar regime prevails at the wave back, $f(\xi_0)$, A and m (defined in [25]) are obtained by [A.3]:

$$f(\xi_0) = (1-\xi_0)^{1/2}(1+2\xi_0); \qquad A = \frac{1}{3}\left(\frac{2\nu}{g}\right)^{1/2}; \qquad m = \frac{1}{2}. \qquad [A.8]$$

Following the derivations outlined in section 2.6, the equilibrium wave celerity in the laminar case is given by

$$3.78 = (1-\xi_0)^{1/3}C\left\{\left[1+3C\left(\frac{(1-2\xi_0)}{(1-\xi_0)(1+2\xi_0)}\right)\frac{d\xi_0}{dC}\right](1+2\xi_0)\right\}^{2/3}. \qquad [A.9]$$

For a prescribed $\xi_0(C)$, [A.9] is solved for $C = C_{eq}$. For instance, $\xi_0 = \text{const}$, yields

$$C_{eq} = 3.78(1-\xi_0)^{-1/3}(1+2\xi_0)^{-2/3} \qquad [A.10]$$

which for $\xi_0 = 0$ yields the result $C_{eq} = 3.78$, previously obtained by Brauner & Moalem Maron (1983) and Brauner (1987).

APPENDIX B

Kinematic Wave Celerity in Turbulent Film

Kinematic waves are quasi-steady-state phenomena. In the particular case of film flow, where the downflow rate is a function of the local film thickness, the kinematic wave velocity describes the propagation of upstream changes in film thickness. The velocity of kinematic waves, V_{wk}, is given by Wallis (1969):

$$V_{wk} = \frac{\partial q}{\partial h} = \frac{\partial\left(\frac{\Gamma}{\rho}\right)}{\partial h}. \qquad [B.1]$$

In a smooth laminar film flow, where $h_N = (3\nu/g\Gamma)^{1/3}$, [B.1] yields $C_k = V_w/V_N = 3.0$. For smooth

turbulent film flow, the relation between the flow rate and film thickness, h_t, is given by (Brauner 1987):

$$\frac{h_t}{\left(\frac{\nu^2}{g}\right)^{1/3}} = \left(\frac{n+1}{4n}\right)^{2n/3(n+1)} S(n)^{1/3}\mathrm{Re}^{2n/3(n+1)}; \qquad \mathrm{Re} = \frac{4\Gamma}{\mu}. \tag{B.2}$$

The corresponding kinematic wave velocity, in a turbulent falling film is obtained by substituting [B.2] into [B.1], which yields:

$$\frac{V_{wk}}{V_t} = \frac{3}{2}\frac{(n+1)}{n}, \tag{B.3}$$

where V_t is the average velocity of the smooth turbulent film, given by

$$V_t = \left(\frac{n}{n+1}\right)\left\{\left[\frac{g}{S(n)}\right]^{n+1}\frac{h_t^{n+3}}{\nu^2}\right\}^{1/2n}. \tag{B.4}$$

The dimensionless kinematic celerity, defined with respect to Nusselt's average film velocity, $V_N(=\Gamma/\rho h_N)$, is given by

$$C_k = \frac{V_{wk}}{V_N} = \frac{3^{4/3}S^{1/3}(n)}{2^{(n+5)/3(n+1)}}\left(1+\frac{1}{n}\right)^{(n+3)/3(n+1)}\mathrm{Re}^{(1-n)/3(n+1)}. \tag{B.5}$$

For $n = 7$, $S(n) = 0.0225$, [B.3] and [B.5] read:

$$\frac{V_{wk}}{V_t} = \frac{12}{7}$$

and

$$C_k = 11.5\mathrm{Re}^{-1/4}. \tag{B.6}$$

Equation [B.6] is identical to [28] with $\xi_0 = 1/3$. Thus, in the limit $\xi_0 \to 1/3$ the equilibrium wave celerity predicted by the turbulent wave model approaches the value derived here for the kinematic wave celerity.